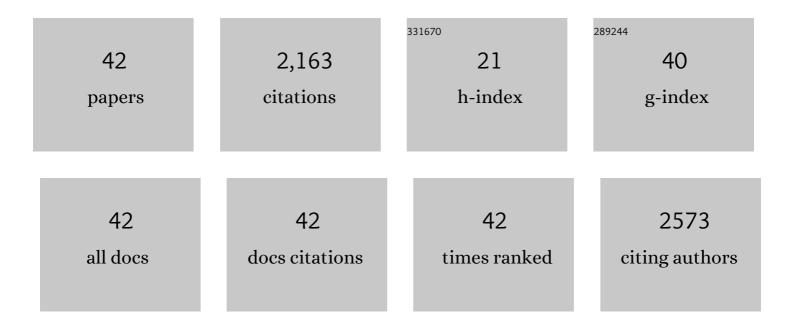
## Sophie Sobanska

List of Publications by Year in descending order

Source: https://exaly.com/author-pdf/3958653/publications.pdf Version: 2024-02-01



#	Article	IF	CITATIONS
1	Foliar Lead Uptake by Lettuce Exposed to Atmospheric Fallouts. Environmental Science & Technology, 2010, 44, 1036-1042.	10.0	342
2	Foliar exposure of the crop Lactuca sativa to silver nanoparticles: Evidence for internalization and changes in Ag speciation. Journal of Hazardous Materials, 2014, 264, 98-106.	12.4	335
3	Copper Oxide Nanoparticle Foliar Uptake, Phytotoxicity, and Consequences for Sustainable Urban Agriculture. Environmental Science & Technology, 2017, 51, 5242-5251.	10.0	203
4	Fate of pristine TiO2 nanoparticles and aged paint-containing TiO2 nanoparticles in lettuce crop after foliar exposure. Journal of Hazardous Materials, 2014, 273, 17-26.	12.4	199
5	Microchemical Investigations of Dust Emitted by a Lead Smelter. Environmental Science & Technology, 1999, 33, 1334-1339.	10.0	133
6	Foliar uptake and metal(loid) bioaccessibility in vegetables exposed to particulate matter. Environmental Geochemistry and Health, 2014, 36, 897-909.	3.4	102
7	Foliar or root exposures to smelter particles: Consequences for lead compartmentalization and speciation in plant leaves. Science of the Total Environment, 2014, 476-477, 667-676.	8.0	93
8	Speciation of PM10Sources of Airborne Nonferrous Metals within the 3-km Zone of Lead/Zinc Smelters. Environmental Science & Technology, 2004, 38, 5281-5289.	10.0	74
9	Investigation of the Chemical Mixing State of Individual Asian Dust Particles by the Combined Use of Electron Probe X-ray Microanalysis and Raman Microspectrometry. Analytical Chemistry, 2012, 84, 3145-3154.	6.5	70
10	Confocal Microprobe Raman Imaging of Urban Tropospheric Aerosol Particles. Environmental Science & Technology, 2006, 40, 1300-1306.	10.0	66
11	Iron Speciation of Airborne Subway Particles by the Combined Use of Energy Dispersive Electron Probe X-ray Microanalysis and Raman Microspectrometry. Analytical Chemistry, 2013, 85, 10424-10431.	6.5	49
12	SEM-EDX Characterisation of Tropospheric Aerosols in the Negev Desert (Israel). Journal of Atmospheric Chemistry, 2003, 44, 299-322.	3.2	45
13	Phytoavailability of lead altered by two Pelargonium cultivars grown on contrasting lead-spiked soils. Journal of Soils and Sediments, 2016, 16, 581-591.	3.0	38
14	TEM-EDX investigation on Zn- and Pb-contaminated soils. Applied Geochemistry, 2001, 16, 1165-1177.	3.0	35
15	Pushing back the limits of Raman imaging by coupling super-resolution and chemometrics for aerosols characterization. Scientific Reports, 2015, 5, 12303.	3.3	35
16	Airborne foliar transfer of particular metals in Lactuca sativa L: translocation, phytotoxicity, and bioaccessibility. Environmental Science and Pollution Research, 2019, 26, 20064-20078.	5.3	33
17	Chemistry at level of individual aerosol particle using multivariate curve resolution of confocal Raman image. Spectrochimica Acta - Part A: Molecular and Biomolecular Spectroscopy, 2006, 64, 1102-1109.	3.9	32
18	Raman diagnostic of the reactivity between ZnSO4 and CaCO3 particles in humid air relevant to heterogeneous zinc chemistry in atmosphere. Atmospheric Environment, 2014, 85, 83-91.	4.1	30

SOPHIE SOBANSKA

#	Article	IF	CITATIONS
19	Synthesis, thermal analysis and crystal structure of lead(II) diaqua 3,6-dicarboxylatopyridazine. Evaluation of performance as a synthetic precursor. New Journal of Chemistry, 1999, 23, 393-396.	2.8	27
20	The fate of Cu pesticides in vineyard soils: A case study using δ65Cu isotope ratios and EPR analysis. Chemical Geology, 2018, 477, 35-46.	3.3	25
21	Single-particle analysis of industrial emissions brings new insights for health risk assessment of PM. Atmospheric Pollution Research, 2018, 9, 697-704.	3.8	23
22	Combined use of quantitative ED-EPMA, Raman microspectrometry, and ATR-FTIR imaging techniques for the analysis of individual particles. Analyst, The, 2014, 139, 3949-3960.	3.5	22
23	Lead distribution in soils impacted by a secondary lead smelter: Experimental and modelling approaches. Science of the Total Environment, 2016, 568, 155-163.	8.0	20
24	Heterogeneous microchemistry between CdSO4 and CaCO3 particles under humidity and liquid water. Journal of Hazardous Materials, 2013, 248-249, 415-423.	12.4	17
25	Is Tillandsia capillaris an efficient bioindicator of atmospheric metal and metalloid deposition? Insights from five months of monitoring in an urban mining area. Ecological Indicators, 2016, 67, 227-237.	6.3	16
26	Tracing the evolution of morphology and mixing state of soot particles along with the movement of an Asian dust storm. Atmospheric Chemistry and Physics, 2020, 20, 14321-14332.	4.9	15
27	Photochemistry of single particles using acoustic levitation coupled with Raman microspectrometry. Journal of Raman Spectroscopy, 2017, 48, 1135-1137.	2.5	14
28	The role of epicuticular waxes on foliar metal transfer and phytotoxicity in edible vegetables: case of Brassica oleracea species exposed to manufactured particles. Environmental Science and Pollution Research, 2019, 26, 20092-20106.	5.3	13
29	Deliquescence behavior of photo-irradiated single NaNO3 droplets. Atmospheric Environment, 2018, 183, 33-39.	4.1	11
30	Hygroscopic behavior of aerosols generated from solutions of 3-methyl-1,2,3-butanetricarboxylic acid, its sodium salts, and its mixtures with NaCl. Atmospheric Chemistry and Physics, 2020, 20, 14103-14122.	4.9	10
31	Combining Raman microspectrometry and chemometrics for determining quantitative molecular composition and mixing state of atmospheric aerosol particles. Microchemical Journal, 2018, 137, 119-130.	4.5	8
32	In Situ Observation of Efflorescence and Deliquescence Phase Transitions of Single NaCl and NaNO3 Mixture Particles in Air Using a Laser Trapping Technique. Bulletin of the Chemical Society of Japan, 2020, 93, 86-91.	3.2	6
33	Combining microscopy with spectroscopic and chemical methods for tracing the origin of atmospheric fallouts from mining sites. Journal of Hazardous Materials, 2015, 300, 538-545.	12.4	4
34	Experimental and theoretical IR study of methyl thioglycolate, CH 3 OC(O)CH 2 SH, in different phases: Evidence of a dimer formation. Journal of Molecular Structure, 2017, 1139, 160-165.	3.6	4
35	An electrochemical method to rapidly assess the environmental risk of silver release from nanowire transparent conductive films. NanoImpact, 2020, 18, 100217.	4.5	4
36	Toward a better understanding of ferric-oxalate complex photolysis: The role of the aqueous/air interface of droplet. Chemosphere, 2022, 289, 133127.	8.2	4

#	Article	IF	CITATIONS
37	Gas-phase and matrix-isolation photochemistry of methyl thioglycolate, CH 3 OC(O)CH 2 SH: Influence of the presence of molecular oxygen in the photochemical mechanisms. Journal of Photochemistry and Photobiology A: Chemistry, 2017, 344, 101-107.	3.9	2
38	Photodegradation of methyl thioglycolate particles as a proxy for organosulphur containing droplets. Physical Chemistry Chemical Physics, 2018, 20, 19416-19423.	2.8	2
39	Experimental and theoretical investigation on conformational and spectroscopic properties of dimethyl dithiodiglycolate, [CH 3 OC(O)CH 2 S] 2. Journal of Molecular Structure, 2017, 1137, 524-529.	3.6	1
40	Influence of collecting substrate on the Raman imaging of micron-sized particles. Analytica Chimica Acta, 2018, 1014, 41-49.	5.4	1
41	Interaction process between gaseous CH <sub>3</sub> 1 and NaCl particles: implication for iodine dispersion in the atmosphere. Environmental Sciences: Processes and Impacts, 2021, 23, 1771-1781.	3.5	0
42	Infrared matrix-isolation and theoretical studies of interactions between CH3I and water. Journal of Molecular Structure, 2021, 1236, 130342.	3.6	0